NANO REVIEWS

COACTION PUBLISHING

REVIEW ARTICLE

# Nanoscale structure, dynamics and power conversion efficiency correlations in small molecule and oligomer-based photovoltaic devices

**Jodi M. Szarko[1], Jianchang Guo[2,3], Brian S. Rolczynski[1,2] and Lin X. Chen[1,2*]**

[1]Department of Chemistry, Argonne Northwestern Solar Energy Research (ANSER) Center, Northwestern University, Evanston, IL, USA; [2]Chemical Sciences and Engineering Division, Argonne National Laboratory, Argonne, IL, USA; [3]Department of Chemistry, James Franck Institute, University of Chicago, Chicago, IL, USA

Received: 28 April 2011; Revised: 27 June 2011; Accepted: 1 July 2011; Published: 12 August 2011

## Abstract

Photovoltaic functions in organic materials are intimately connected to interfacial morphologies of molecular packing in films on the nanometer scale and molecular levels. This review will focus on current studies on correlations of nanoscale morphologies in organic photovoltaic (OPV) materials with fundamental processes relevant to photovoltaic functions, such as light harvesting, exciton splitting, exciton diffusion, and charge separation (CS) and diffusion. Small molecule photovoltaic materials will be discussed here. The donor and acceptor materials in small molecule OPV devices can be fabricated in vacuum-deposited, multilayer, crystalline thin films, or spin-coated together to form blended bulk heterojunction (BHJ) films. These two methods result in very different morphologies of the solar cell active layers. There is still a formidable debate regarding which morphology is favored for OPV optimization. The morphology of the conducting films has been systematically altered; using variations of the techniques above, the whole spectrum of film qualities can be fabricated. It is possible to form a highly crystalline material, one which is completely amorphous, or an intermediate morphology. In this review, we will summarize the past key findings that have driven organic solar cell research and the current state-of-the-art of small molecule and conducting oligomer materials. We will also discuss the merits and drawbacks of these devices. Finally, we will highlight some works that directly compare the spectra and morphology of systematically elongated oligothiophene derivatives and compare these oligomers to their polymer counterparts. We hope this review will shed some new light on the morphology differences of these two systems.

Keywords: *organic photovoltaics*; *perylene*; *thiophene*; *charge transport*; *transient absorption*; *grazing incidence x-ray scattering*

**Jodi M. Szarko** received her B.A. from Wesleyan University and her Ph.D. from the University of Colorado at Boulder. After working at the Helmholtz Centrum Berlin, she is currently a Postdoctoral Researcher at Northwestern University. Her main focus is on the structural and kinetic properties of organic photovoltaics.

**Dr Jianchang Guo** conducted his PhD, M.S. and B.S. at Emory University (USA), Dalian Institute of Chemical Physics (China), and Xiangtan University (China), respectively. He is currently a Postdoctoral Fellow in the Chemical Science Division of Oak Ridge National Laboratory, USA. Jianchang's research interests include applications of ultrafast laser spectroscopy in polymer solar cell, super-capacitors and Li-ion battery materials.

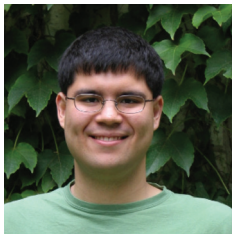

**Brian S. Rolczynski** received his BA in English and his BS in Chemistry at the University of Washington. He is currently a graduate student at Northwestern University studying the spectral and dynamic properties of systematically altered low band-gap copolymers.





Citation: Nano Reviews 2011, **2:** 7249 - DOI: 10.3402/nano.v2i0.7249

The photovoltaic effects and photoconductivity in organic materials have been studied extensively for decades (1–5), and, as a result, the mass production of organic solar cells is well within our reach. Collaborative efforts in such an interdisciplinary field have greatly improved our understanding of the fundamental processes occurring in these devices: (1) light harvesting, (2) exciton diffusion, (3) CS, (4) charge carrier diffusion, and (5) charge collection. These fundamental processes (Fig. 1) occur in both (a) multijunction and (b) bulk heterojunction solar cells. While all of these processes affect the overall device power conversion efficiency (PCE), only the first three processes are discussed in this review. The PCE is calculated by measuring the open circuit voltage ($V_{OC}$) and the short circuit current ($J_{SC}$) of solar cell devices, and by calculating the fill factor (*FF*), which is the ratio of the maximum device power divided by the power calculated by the product of $V_{OC}$ and $J_{SC}$. The PCE ($\eta$) is then expressed as $\eta = \frac{V_{oc} J_{sc} FF}{A \cdot I}$, where $I$ is the total light intensity and $A$ is the illuminated area of the device. The external quantum efficiency ($\eta_{EQE}(\lambda)$) is related to $J_{SC}$ by $\eta_{EQE}(\lambda) = \frac{J_{sc}(\lambda)/e}{I(\lambda)\lambda/hc}$, where $J_{SC}(\lambda)$ is the incident wavelength ($\lambda$) dependent short-circuit current, $e$ is the elementary charge, $I(\lambda)$ is transmitted monochromatic light at $\lambda$, $h$ is Planck's constant, and $c$ is the velocity of light in vacuum. The $\eta_{EQE}(\lambda)$ can also be expressed by the efficiencies of individual processes listed above:

$$\eta_{EQE} = \eta_A \eta_{ED} \eta_{CS} \eta_{CT}, \quad (1)$$

where $\eta_A$, $\eta_{ED}$, $\eta_{CS}$, and $\eta_{CT}$ are efficiencies for the light absorption, exciton diffusion, CS, and charge transport and collection processes, respectively (6). When the efficiency for each process is optimized, the device PCE is maximized. Interestingly, the first of these processes, light harvesting/absorption, is one of the parameters in organic photovoltaics (OPV) that has not been improved significantly until recent years, and more improvements are still in progress. The first solar cells had a relatively narrow overlap between their absorption profile and the solar spectrum, whereas conjugated conducting molecules with a smaller optical gap developed in recent years have very wide absorption spectra in the visible region, which is one of the main improvements in the enhancement of $\eta$.

In contrast, one of the first issues effectively tackled in OPV cell production was the CS. Although the photoconductive effect on these materials was studied as early as the 1950s (7), the first truly viable organic solar cell with small molecules was not developed until 1985 (1). The generation of photocurrent and voltage using a bilayer p/n junction made from small molecule films was a revolutionary breakthrough. An electron donor forms the first layer and is photoexcited to create an exciton that subsequently diffuses to the bilayer junction, where the electron can hop to the electron acceptor, which makes up the second layer in the device. The exciton splitting at the junction creates two well-separated charge carrier species: the electron and the hole (Fig. 1). This concept has proven to be the best suited for interpretation of OPV effect and is widely accepted in almost all solar cell device design today.

Although the molecular bilayer p/n junction has established potential for the OPV effect in solar cell applications, the PCE at that time was still below 1% because this device architecture was not optimized for interfacial CS and interactions between the electron donor and acceptor. The quality of each material individually will affect both the exciton and charge carrier diffusion in the films. Exciton diffusion has been a serious bottleneck for many years in OPV systems compared to their inorganic counterparts. Because of the disorder in organic materials, the exciton diffusion length is orders of magnitude smaller ( ~10 nm) compared to conventional inorganic solar cell materials, such as silicon, which can have diffusion lengths over 100 microns (8). Because exciton diffusion lengths in organic materials can be many times smaller than their optical absorption lengths, maximizing the light harvesting capabilities by making thicker bilayer cells is often detrimental to the exciton diffusion efficiencies, while thinner cells will increase the exciton diffusion efficiency but lower the light harvesting efficiency. Therefore, an overall optimal efficiency must be achieved that balances light harvesting and exciton diffusion. In order to have effective CS and charge carrier generation, the prerequisite for photon-to-electron/hole conversion is for excitons to migrate quickly to

**Lin X. Chen** is Senior Chemist in Argonne National Laboratory and Professor of Chemistry at Northwestern University. Her research is currently focused on ultrafast transient molecular structural studies in solar energy conversion processes and structures–dynamics–efficiency correlations in organic photo- voltaic materials using ultrafast laser and X-ray spectroscopies and X-ray structural characterization. She received her BSc and PhD degrees from Peking University in China and the University of Chicago, respectively. Her group website is at http://chemgroups.northwestern.edu/ chen_group/.



Citation: Nano Reviews 2011, **2**: 7249 - DOI: 10.3402/nano.v2i0.7249

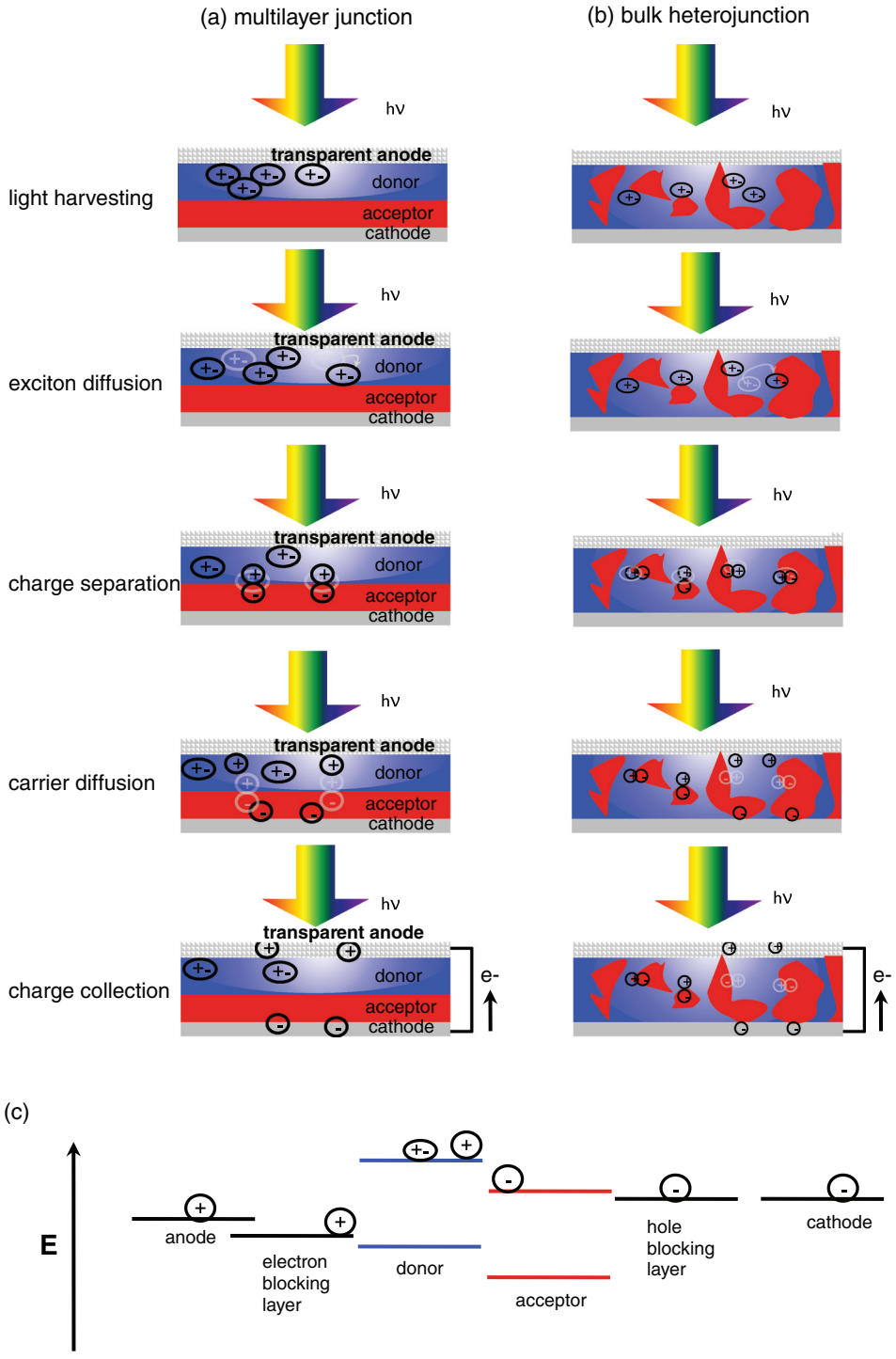


*Fig. 1.* (a) Carrier generation and transport in a two layer junction. First, excitons are created upon light excitation (light harvesting). Some of the excitons then diffuse through the donor (or, in some cases, the acceptor) material and reach the donor acceptor material (exciton diffusion). Once the excitons reach the donor acceptor interface, the potential energy difference of the electronic states of the two materials provides a driving force for the electrons in the excitons of the donor material to transfer to the acceptor material (charge separation). Finally, the separated charges diffuse back to their respective electrodes, where these charges are collected (carrier diffusion and charge collection). (b) Carrier generation and transport in a bulk heterojunction (BHJ) device. The same five processes are necessary for efficient photocurrent generation. In the two layer junction device, the largest bottleneck in the PCE is the exciton diffusion mechanism while the optimization of BHJ devices focuses on improving the carrier diffusion process in these blended films. (c) An energy schematic of the donor-acceptor OPV motif.

the donor:acceptor junction before they decay back to the ground state. If the exciton diffusion lengths are too small, the CS in these materials will be inefficient, which will in turn affect the overall PCE. Therefore, the distance between the donor and acceptor materials needs to be relatively small, or the diffusion length of the excitons needs to be enhanced. The film thickness cannot simply be lowered to the exciton diffusion length of these materials or the light harvesting effects will be diminished.

The fabrication of bulk heterojunction materials via spin casting methods was first used in 1995 to optimize both the light harvesting and exciton diffusion conditions (2). By depositing the donor and acceptor materials simultaneously, the average segregated domain size of the donor and acceptor materials is reduced, making the distance for the exciton travelling to the donor/acceptor boundary sufficiently short and CS efficiencies higher compared to the molecular bilayer devices. While the films prepared by this method, known as bulk heterojunction (BHJ) films, have efficient exciton diffusion, the smaller crystalline domain sizes also degrade the overall crystalline quality of the domains. This crystal degradation can have adverse effects on the carrier migration through the materials, which occurs after CS. The presence of both crystalline and amorphous materials leads to a combination of complicated 'exciton hopping' and 'random walk' components of the charge migration (9), which is not as efficient as a well-ordered crystalline diffusion. Therefore, there have also been several investigations into increasing the crystallinity and diffusion length of the organic materials used in solar cell devices (5). By increasing the diffusion length of the materials, the limit imposed on the domain sizes by this property can also be increased, which will give more order in the charge migration and exciton diffusion of the films. The interplay of the maximum interface area for CS and the optimal crystallinity for charge migration lies at the heart of solar cell optimization today. This interplay is greatly affected by the active film morphologies. As a consequence to optimize these two characteristics, there have been two main veins of organic solar cell research: (1) small molecule and oligomer materials and (2) conjugated oligomer and polymer materials blended with buckminsterfullerene derivatives.

Organic solar cells are typically made by vapor deposition, which produces more ordered layers, or spin coating, which produces BHJ films and can be annealed to improve crystallinity. Spin casting is ultimately more inexpensive and scalable compared to vapor deposition methods, while vapor deposition allows for a higher degree of morphological control. As the processing conditions for organic solar cell devices continues to improve, some overlap and refining of the aforementioned film production methods has occurred. For instance, vapor deposited solar cells can contain neat or blended film layers and the optimized blended film morphology for various devices can be crystalline, nanocrystalline, or amorphous (10, 11). Some preparations have utilized both spin casting and vapor deposition methods (12). In November 2010, the highest efficiency of both small molecule and polymer solar cells reached an efficiency of 8.3% (13, 14). The small molecule devices were vapor deposited while the polymers were spin cast from solutions. Some materials, such as oligothiophene derivatives, can be processed using either vapor deposited or spin casting methods. These materials have recently shown promise in creating high efficiency OPV cells, and they also serve as a representative system to study the physical processes in the materials to better understand the mechanisms leading to enhanced solar cell efficiencies. In this review, we will first discuss the optimal qualities and state of the art of materials used in small molecule and oligomer solar cells. We will then discuss some of our current findings of systematically elongated thiophene oligomer materials and their spectral and morphologic properties. Finally, we will compare the morphology and transient absorption spectroscopy of an oligomer species, MF, and its polymer counterpart, PF.

## The evolution of device optimization in small molecule OPV materials

### *1. Phthalocyanines: a first case study in organic photovoltaic (OPV) materials*

The first organic solar cells created were based on phthalocyanine (Pc) and perylene (PER) derivatives (1). Their structures are shown in Fig. 2. The Pc electronic properties have been extensively studied for several reasons: Pc structures are similar to those of chlorophyll naturally occurring in photosynthetic membrane proteins. These relatively large, planar, conjugated molecules have intense absorption bands in the UV-vis region, and are capable of donating electrons from their excited states to the LUMO of the PER acceptor material. The first single heterojunction solar cells were made of Pc as the electron donor layer and had a PCE of $<1\%$. In the past 25 years, considerable molecular engineering and film quality investigations have led to a significant increase in the overall device PCE. Two breakthroughs developed using Pc materials have been instrumental to the improvement of many different small molecule and polymer photovoltaic devices. One breakthrough was the addition of an 'electron blocking layer' between the acceptor and the cathode (15), preventing organic film damage during the evaporation of the cathode layer and directing the excitons' diffusion to the junction, which in turn increases the CS. A schematic of the energy levels of an organic solar cell with this blocking layer is shown in Fig. 1c. The second breakthrough, which is currently where the main thrust of organic electronic



Citation: Nano Reviews 2011, **2**: 7249 - DOI: 10.3402/nano.v2i0.7249

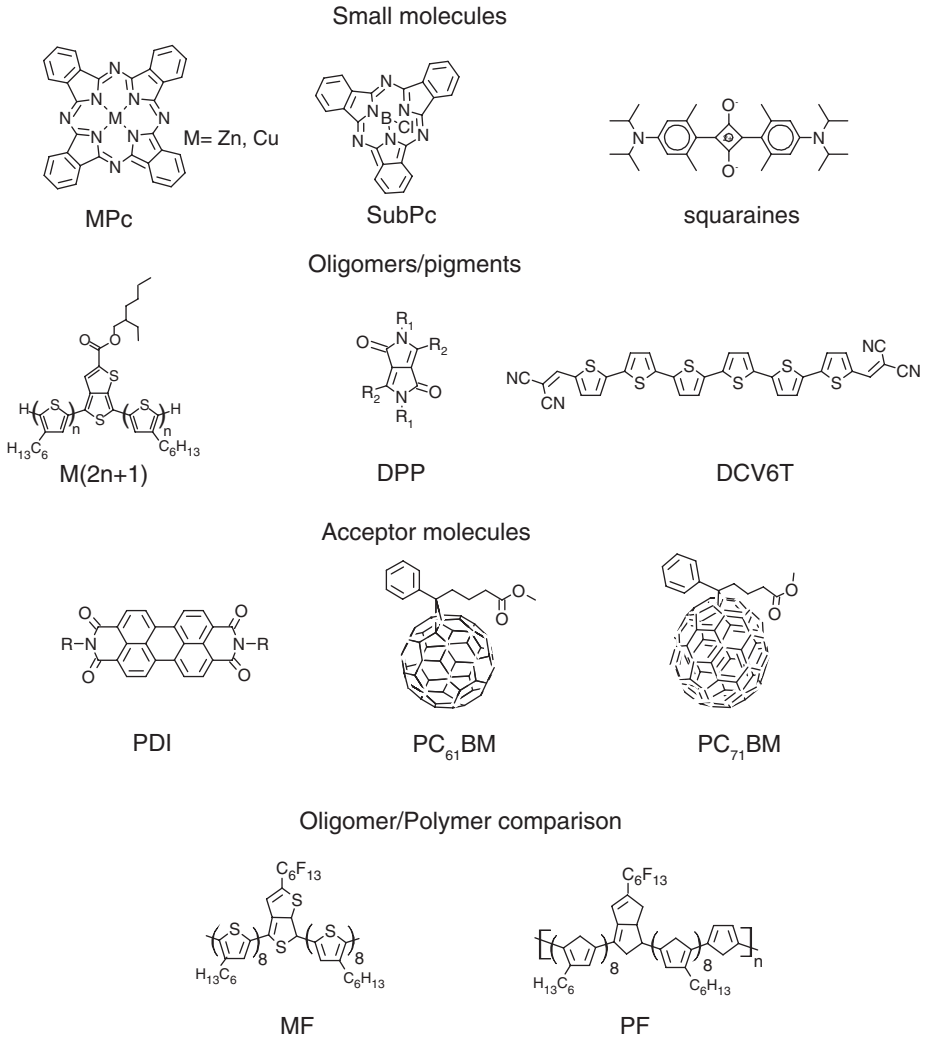


*Fig. 2.* The molecular structure of the species discussed throughout this review.

research still lies, is in increasing the interaction area or junction area between the donor and acceptor materials. There have been several methods employed to achieve this goal, such as the co-depositing of donor and acceptor materials (16, 17) and the production of 'graded heterojunction' materials by systematically changing the ratio of the donor and acceptor materials being deposited onto the substrate (18). The delicate interplay of film crystallinity and donor:acceptor interface optimization has been the subject of many investigations and is still undergoing improvements as our understanding of film morphology increases.

Although the investigations of Pc-based solar cells have produced a wealth of understanding and improvement of these devices, there are drawbacks in using Pc materials for OPV devices. The main drawbacks are the overlap of the Pc absorption (Fig. 3) with the solar spectrum and the energy level alignment between the donor and acceptor materials for the CS. Compared to the spectrum of the sun, the Pc absorption spectra with two intense but narrow absorption peaks can only allow these materials to harvest a very limited amount of solar photons. In order to circumvent this limit, many Pc derivatives have been synthesized to broaden the absorption spectra in order to increase the light harvesting efficiency (19). Chemical synthesis, as well as film fabrication engineering, can also optimize the alignment of the Pc HOMO and LUMO levels with respect to the acceptor materials. The second parameter that is less than ideal for these materials is the film characteristics (20). Due to their planar structure, many Pc polymorphs have been observed in the literature (21) due to many weak intermolecular interactions, affecting the film morphology and stability. Furthermore, a large number of Pcs are insoluble in most solvents, so the materials can only be created using the expensive vapor deposition rather

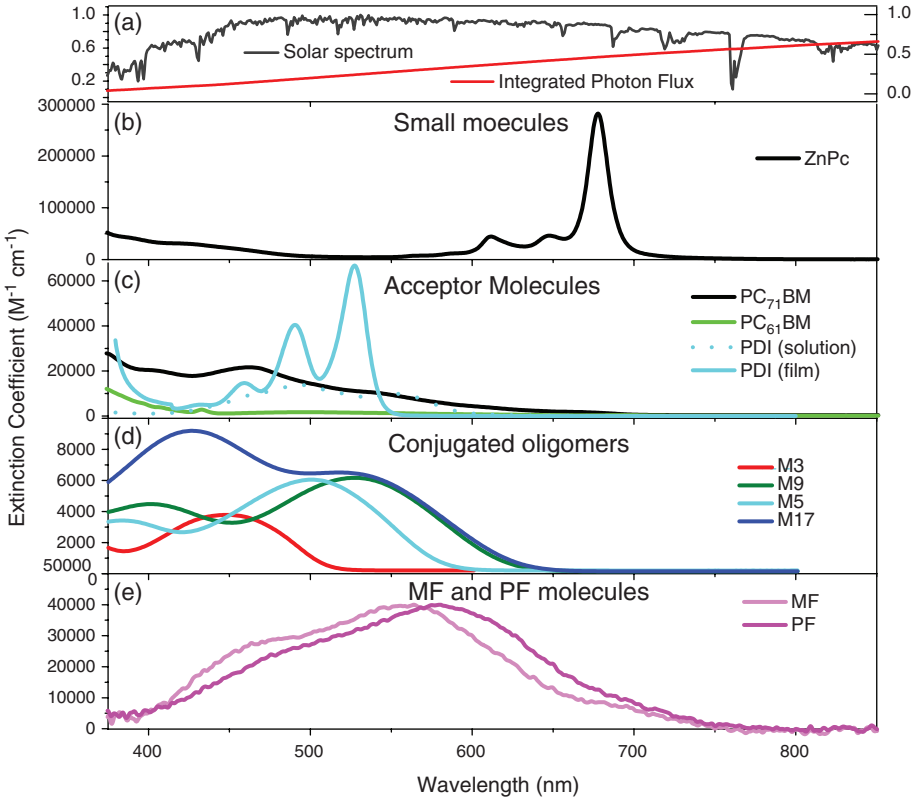


*Fig. 3.* (a) The Solar absorption AM 1.5 spectrum and the corresponding integrated photon flux taken by integrating this spectrum. (b) The absorption spectrum of phthalocyanine compounds. These compounds have a high extinction coefficient, but they do not have a wide absorption band. (c) The absorption spectrum of $PC_{61}BM$, $PC_{71}BM$, and a perylene diimide derivative. (d) The absorption spectrum of a systematically altered conjugated oligomer series. The oligomers M3, M5, M9, and M17 are shown here. (e) The absorption spectrum of the oligomer MF and its corresponding polymer PF.

than spin casting (22). Some efforts have been made to make soluble Pc materials (23), but they have not been very successful. The use of a new Pc derivative, boron sub-Pc (sub-Pc) (Fig. 2), has helped in solving the issues of band level alignment and film morphology (24, 25). The $V_{OC}$ of the sub-Pc device is larger when prepared with conventional solar cell acceptor materials, and the PCE is consequently higher compared to the corresponding Pc-based devices. The sub-Pc molecules have a $C_3$ symmetry, rather than a $C_4$ symmetry in Pc, and their less planar structures make them more soluble in common solvents and hence easier processing than Pc materials. The lower order symmetry also makes the molecules more susceptible to changes in film morphology due to growth conditions. Currently, the highest efficiency Pc solar cells use these sub-Pc derivatives in a graded heterojunction morphology. The efficiency of a single heterojunction device is 4.2% (18).

### 2. OPV materials based on squaraines: increasing the energetic overlap with the solar spectrum

In spite of progress in using Pc OPV materials in the past 25 years, there is still room for improvement in the small molecule-based OPV devices, such as using different types of small molecule materials for higher solar cell efficiencies. Squaraines (Fig. 2) are one series of the materials as alternative of Pcs. There are three main reasons why squaraines were initially investigated as potential electron donors in organic solar cell devices (26, 27). The first was the increased overlap of their absorption spectrum with the solar spectrum. These molecules have an internal donor-acceptor character, which in turn lowers the bandgap of the material. The donor-acceptor character of these molecules can also enhance the CS of the excitons in these devices. The absorption spectrum is also significantly broadened in films, further enhancing the absorptive overlap with the solar spectrum and the light harvesting efficiency in solar cell devices. The second reason for studying squaraines is that the HOMO energy levels of these molecules are relatively low, so a sufficiently high open circuit voltage can be maintained while lowering of the bandgap (21). Moreover, the squaraines films have significant crystallinity due to strong interactions between squaraine molecules, which will enhance the carrier transport in these films (12, 28). The stacking distance



Citation: Nano Reviews 2011, **2**: 7249 - DOI: 10.3402/nano.v2i0.7249

between squaraine molecules in a film is approximately 3.4 Å (27). This densely packed structure facilitates carrier transport and also further broadens the optical absorption spectrum. The feasibility of spin casting squaraine thin films minimizes the production cost of solar devices using these materials. Squaraine films have been made using both vapor deposited and spin casting methods (12, 26). The highest efficiencies for single heterojunction devices has been achieved by using squaraine derivatives and a combination of vapor deposited and spin casting methods. Efficiencies as high as 5.2% have been reported (29). Therefore, it is expected that the study of squaraine films in OPV devices will remain as an intense area of study in future works.

### 3. Perylene derivatives: systematically controlled acceptor materials

Small molecule acceptor materials are typically used in both vapor deposited and spin cast devices. Two acceptor materials have been used extensively in the past, PER and buckminsterfullerene derivatives, which are highlighted below. Although other materials are being investigated as electron acceptors in organic films, their properties lie outside the scope of this review. The first electron acceptor material utilized in OPVs was a PER derivative (see Fig. 2). These were the first set of molecules to show the n-type electronic character necessary for electron acceptor materials. As an added benefit, these compounds are well known to have a very high degree of crystallinity when incorporated into films. Therefore, most initial works were performed on this compound (30). This higher degree of crystallinity led to the assumption that the exciton diffusion length is very large for most PER derivatives. In fact, these molecules have only a moderate diffusion length of $\sim$3 nm (31). Although the exciton diffusion length is relatively small for PER derivatives, there are still many investigations into the potential use of this material in organic solar cells due to their high electron mobility in solid films. Although the exciton diffusion length of PER derivatives is not significantly enhanced by the superlative crystal packing, the charge carrier diffusion length is enhanced. The highest efficiency solar cells require a delicate balance of exciton diffusion and carrier transport optimization. capitalized, such as PTDCA and PPEI, are potentially promising materials that have an exciton diffusion length as large as 88 nm (31). Perhaps the most challenging issue in these small pigment molecule-based OPV materials is to form an optimal morphology through self-assembly to significantly control the CS dynamics in these films (32, 33). In particular, one would like to tailor the materials so that the controlled self-assembly via intermolecular interactions can be achieved to form dual continuous channels respectively for the donor and acceptor for the carrier transport while the donor and acceptor are covalently linked (32–36). Perylene is an ideal electron acceptor in this application. The planarity of the molecule will facilitate favored self-aggregation in these films. The improvement of the bound pair devices demonstrates the huge potential this approach offers and further enhancement is expected by optimizing processing and post-production treatments.

### 4. Buckminsterfullerene derivatives: more ideal electron acceptor materials

Around the same time that the first single heterojunction solar cells were being produced, the buckminsterfullerene molecule ($C_{60}$) was also discovered (37). This revelation led to an explosion of interest on the chemical, optical, and electronic properties of the material. In particular, the conductivity of $C_{60}$ was quickly established, and the use of this material in electronic applications such as OPVs became an emerging field of study (4). One attractive feature of $C_{60}$ is its long electron diffusion length. To increase the overall PCE of the perylene-based devices, a material with an increased electron diffusion length is required. The reported exciton diffusion length of the acceptor material $C_{60}$ is substantially longer compared to PER derivatives such as PTCBI, which is attributed to the rapid intersystem crossing of the singlet excited state to the long-lived triplet excited state allowing ample time for its diffusion (31). In single heterojunction devices with narrow absorption bands, the exciton absorption in the acceptor material can significantly affect the overall solar cell efficiency. The absorption spectrum of $C_{60}$ is shown in Fig. 3. The initial experiments on solar cell devices used polymers as the active donor material were initiated in 1993 (38). It was not until 2001 that PER was substituted by $C_{60}$ for single heterojunction small molecule devices (39). One reason for the lag time of using $C_{60}$ in vapor deposited small molecule devices was the concern that the relatively small extinction coefficient of $C_{60}$ would lower the light harvesting efficiency and hence the device PCEs. Compared to Pc and PER derivatives whose extinction coefficients are in $10^4$–$10^6$ $M^{-1}cm^{-1}$, $C_{60}$ has an extinction coefficient of only $10^3$ $M^{-1}cm^{-1}$ in the visible spectral region (40). Although the extinction coefficient is lower for $C_{60}$ compared to PTCBI, the longer diffusion length and therefore the exciton diffusion efficiency, overcompensates for the reduced light harvesting efficiency in $C_{60}$. The films can also be made thicker, which will enhance the light harvesting. Therefore, replacing PTCBI with $C_{60}$ increases the *EQE* for wavelengths within the $C_{60}$ absorption band.

Another reason for the long lag time of the fullerene derivative in small molecule solar cells is the initial low power conversion efficiencies of the material. The first fullerene derivative solar cells, which were used with

polymer donor materials, had efficiencies lower than 0.1% (38). This low efficiency was attributed to the poor donor-acceptor interface of the material. A revolutionary breakthrough in the field of OPVs occurred when a derivative of $C_{60}$, [6,6]-phenyl-$C_{61}$-butyric acid methyl ester (PCBM), was synthesized in 1995 (41). This material is more soluble compared to the unsubstituted fullerene. The high solubility of this material led to the fabrication of the bulk heterojunction (BHJ) films, which enhance the interfacial interactions between the donor and the acceptor (2). Since then, this material and its derivatives have been used almost exclusively in polymer solar cell devices.

The low absorption of $C_{60}$ derivatives in the visible and infrared spectrum can be attributed to a high degree of symmetry, making the lowest-energy transitions formally dipole forbidden. Therefore, when the $C_{60}$ moiety, $PC_{61}BM$ is replaced by a less symmetrical or elliptical fullerene, $PC_{71}BM$, these transitions will become allowed and a dramatic increase in light harvesting is expected. The use of $C_{70}$ and $PC_{71}BM$ has been shown to increase solar cell efficiencies (42). The absorption spectrum of $PC_{71}BM$ is also shown in Fig. 3. The enhanced absorption over the entire visible range increases the overall short circuit current in the film devices. The electronic band level alignment is very similar for $C_{60}$ and $C_{70}$ derivatives (43), so the open circuit voltage and fill factors are similar for the two kinds of devices. Therefore, the PCE in many solar cell devices has been enhanced by using $C_{70}$ derivatives as the acceptor material. Nevertheless, $C_{60}$ is still often used as the acceptor material for comparative purposes or in devices where the donor material has a high extinction coefficient over the entire visible spectrum. The $C_{70}$ derivatives are more difficult and expensive to separate, so $C_{60}$ is used in cases where the increase in the efficiency does not increase significantly using $C_{70}$ derivatives. The production of other fullerene derivatives, such as indene-substituted fullerenes, continues to increase solar cell efficiencies (44).

## 5. Oligothiophene derivatives: a new avenue in OPV donor material optimization

Oligothiophene derivatives have been studied for a wide array of organic electronics and have shown much promise in field effect transistors in past years. They have high hole mobilities and the charge carrier mobility can, in turn, ensure high carrier transport in these materials. One of the main reasons why these materials are not favorable for solar cell devices is the very high bandgap of these small molecule materials. Early works on small molecule bulk heterojunction solar cells were focused on branched oligothiophenes (45). More recently, there have been substitution methods employed to lower the bandgap of these materials (46). Promising results have recreated recent interest in the investigation of oligothiophene derivatives as a potential donor material in BHJ solar cells. Some results are highlighted below.

Representative structures of three conjugated aromatic oligomers and fused aromatic ring derivatives are shown in Fig. 2. The number of these kinds of systems studied for the purpose of OPVs is actually quite extensive. For arrays of small molecule organic systems developed in the past, the reader is directed to previous reviews (47). Because of the limited scope of this review, only two specific systems will be discussed in detail here, representing the current state-of-the-art materials for organic oligomer photovoltaics. Essentially, the improvement of these materials has been focused on the optimization of four main properties: (1) the reduction of the bandgap, (2) the improvement of the film structure, (3) the enhancement of solubility for easier film production, (4) the increase in electron affinity to yield high open circuit voltages and device stability (48–50).

There is an enormous number of chemicals produced for use as dyes and pigments, many of which have been investigated for OPVs applications. These molecules have several advantages over larger molecular materials because they are small, exhibit self-assembly, and are easily modified and processed. Pigment chemistry is a well-established field and has produced many commercially available products with long-term stability and low production costs. For organic solar cells, pigments can be optically tuned to desired spectral characteristics, such as maximizing the spectral overlap with the solar spectrum. These molecules have been fabricated to be easily substituted, so fine tuning their properties is a fairly straightforward process. For instance, by the addition of structurally or electronically viable side groups, the film morphology or band level alignment can be controlled. One particular group of pigments that has been modified to create very high efficiency small molecule bulk heterojunction (SMBHJ) solar cells contains a 3,6-diaryl-2,5-dihydro-pyrrolo-[3,4-c]pyrrole-1,4-dione (DPP) central unit (Fig. 2) (49, 51, 52). The DPP unit lies in the center of this molecule. The optical properties of the molecule can be altered by attaching electron donating aromatic side chains such as thiophene (TH), furan, or phenyl groups. Aliphatic side chains can be added at the nitrogen atoms in order to optimize the film morphology and solvent solubility. The central DPP unit also lowers the relative energy levels, which increases the open circuit voltage and stability in these devices. In short, these pigments have shown superlative outputs for all of the four properties mentioned above. Therefore, these molecules have proven to be very promising in the field, and efficiencies as high as 4.4% have been reported for these devices (51). This is the highest efficiency for a completely solution processed small molecule single cell reported to date. Due to the modular nature of this molecular system, the side chains



Citation: Nano Reviews 2011, 2: 7249 - DOI: 10.3402/nano.v2i0.7249

can be systematically altered in future works to improve device characteristics even further.

In particular, the addition of cyanovinylene moieties to the oligothiophene units creates donor:acceptor character within the oligomer, which in turn lowers the bandgap of the material. An example of such an oligomer is shown in Fig. 2. There have been many studies on the dependence of the oligomer length and number of cyanovinylene units on the oligomer to study the optimal electronic properties for this material (53). Cyanovinylene additives are promising side groups because they lower the optical bandgap by lowering the LUMO level of the oligothiophene while the HOMO level remains fairly constant (54). These units act as electron acceptors while the oligothiophene acts as an electron donor, which puts these oligomers in the 'push-pull chromophore' category. The oligomer shown in Fig. 2, DCV6T, has shown the best efficiencies for OPV devices. The HOMO and LUMO levels are at −5.22 eV and −3.44 eV, respectively (55). Compared to unsubstituted or alkyl substituted sexithiophenes, whose HOMO and LUMO energy levels lie at −5.3 eV and −3.0 eV, respectively (56), the HOMO level of DCV6T is constant while the LUMO energy position is reduced. The addition of two cyano units to each vinylene side chain, as is shown for the DCV6T molecule, creates the optimal electronic structure. One cyano end unit does not significantly lower the LUMO level while three cyano units lower the bandgap and energy levels so far that the material can no longer act as a p-type electron donor and has actually been studied as an n-type electron acceptor in OPV applications. For vapor deposited single cell devices, PCEs as high as 4.9% have been reported (57). A similar dicyano oligothiophene, DCN7T, has shown efficiencies as high as 3.7% in solution cast films (58). The high efficiencies are due to the combination of the structural and electronic properties of the material. A p-i-n tandem solar cell containing two vertically stacked solar cells (one cell containing ZnPc:PCBM and one cell containing DCV6T:PCBM as the active layer) has been thoroughly analyzed and PCEs close to 6% were reported (59). The devices also exhibit very high long-term stability. The same authors have very recently reported a tandem solar cell efficiency of 8.3% (13). Although the exact device structure has not yet been reported, these cells presumably contain the same active materials. These solar cells have also been prepared industrially so they are very close to the mass production stage.

Although the field of oligothiophene OPV devices is not investigated as widely as their polythiophene counterparts, they have very recently shown some promising results regarding their device efficiencies. Furthermore, a wide variety of information can be determined by studying oligomer species. These systems can be more systematically regulated, which can in turn improve our understanding of the physical properties of these molecules. In some of our previous studies (60, 61), four co-oligomers were synthesized, each of which consists of one thieno[3,4-*b*] thiophene derivative (TT) unit at its center linked at both ends with one hexyl oligothiophene fragment attached on either side. The oligothiophene fragments were symmetric and were 1, 2, 4, or 8 thiophene units in length. The co-oligomers were, hence, named M3, M5, M9, and M17 with their numbers corresponding to the total monomer units in the co-oligomers. The structural schematic for these molecules is shown in Fig. 2. A fluorinated analog of the M17 molecule, MF, and it corresponding polymer, PF, were also synthesized and are shown in Fig. 2 (62). With these systems, we systematically characterized both electronic and intrachain structural effects arising from the addition of the fused ring in the TT unit to these co-oligomers. The spectral, structural, and kinetic details of these materials are highlighted in the section below.

## Specific case studies

The studies outlined below compare spectral, structural, and temporal characteristics of conducting polymer and oligomer species related to their applications in photovoltaic devices. We highlight our investigations on one oligomer series, the 'M series oligomers' (Fig. 2, M($2n+1$)). These results give meaningful insight on the interplay between the various parameters in these photovoltaic materials and their influences on device performance. Comparative studies were also carried out on benchmark systems such as oligothiophenes and poly-3-hexylthiophene (P3HT).

### *1. The 'M series' oligomers: co-oligomers with a central thienothiophene attached to oligothiophenes of various lengths*

#### *1.1. Spectral effects: systematic control of the optical bandgap*

The main motivation for this oligomer comparison work was to systematically investigate the range of electronic effects from a single unit in a conjugated backbone in oligomers (60), to characterize the thin film morphology of these oligomers (61), and to optimize the overlap of the oligomer absorption with the solar spectrum. These co-oligomers share a common central (TT) unit, but differ with the number of TH side units attached (Fig. 2). The direct connection of the TT unit with higher electron affinity with those of TH units of lower electron affinity is the approach used in construction: efficient light harvesting charge transfer copolymers for solar cell materials. However, the details of how the two or more kinds of units interact along the conjugated backbone are not clear. This series of co-oligomers serve as models for

our understanding of electronic effects propagating from a single TT unit along a π-conjugated backbone.

First, the spectral effects of lengthening the TT oligomer units were investigated as a means to optimize the collection efficiency in these materials. The steady-state absorption spectra are shown in Fig. 3 for the M3, M5, M9, and M17 molecule in toluene solutions. The absorption peaks red-shift as the oligomer length increases, which suggests that the electron delocalization length in the excited state increases with the oligomer size. There were also two electronic peaks present in the absorption spectrum. The lower energy peak, denoted as S1, was attributed to a pseudo charge transfer state. The electron density is pulled from the TH oligomers toward to the central TT unit. As the number of TH units increases by an increment of two units on each side of the TT unit, the amount of red-shift decreases. The S1 peak position has only a slight red-shift in the M17 spectrum compared to that of M9, suggesting an obvious saturation of the red-shift as a function of the length. The S1 peak for the longest oligomer M17 was at 2.31 eV (535 nm), which was 0.45 eV lower than the lowest energy peak of the P3HT absorption spectrum in solution at 2.76 eV (450 nm) (63, 64). This result clearly indicates the significant effect of a single TT unit in lowering the bandgap of the oligomer due to the nature of this pseudo charge transfer state. The question, therefore, is what the optimal number of TT units would be for the highest possible efficiency photovoltaic with multiple factors considered.

We investigated the effects of the TT unit on the exciton diffusion length by determining the conjugation length of this series. In order to more accurately determine the conjugation length of the lower energy S1 state, the relationship between the optical bandgap and the oligomer backbone units was determined. It is well known that for longer oligomers, the optical bandgap of the material can become saturated, which then follows the relationship (65):

$$E(n) = E_\infty + (E_1 - E_\infty)\exp(-s(n-1)), \quad (2)$$

where $E_\infty$ is limiting optical bandgap for $n \to \infty$, $E_1$ is the energy of the monomer, $s$ is a parameter related to the saturation length of the molecule, and $n$ is the number of monomer units. The $s$ was determined to be $0.54 \pm 0.02$ from the absorption and the fluorescence spectra, which suggests that the oligomers investigated in this work reached over 95% spectral shift saturation within seven monomer units. The effective conjugation length (ECL) is defined as the smallest number of units in which the optical bandgap differs by less than 1 nm compared to the limiting optical bandgap (in nm). Using the relationship above, the ECL for the S1 state is 11 units. In contrast, the ECL for benchmark oligomers such as oligothiophene is 17–20 units (65). Therefore, we concluded that the ECL for the M series oligomers was shortened by a factor of two compared to the unsubstituted hexyl-oligothiophenes. Nevertheless, the ECL of the S1 state was surprisingly long considering the electronic state was formed by the effects of a single TT unit.

### *1.2. Morphology dependence: intermolecular packing of the oligothiophene and thienothiophene side chains*

When the aforementioned oligomers are used in photovoltaic materials, they will be processed into thin films. It has been commonly acknowledged that the film morphology, namely their domain size and crystallinity, can significantly influence the photovoltaic device performance (66). In order to better understand the film morphologies and their difference on oligomers of varying length, atomic force microscopy (AFM) and grazing incident x-ray diffraction (GIXRD) measurements were carried out on the M series oligomers to probe molecular packing in these self-assembled architectures at different levels, from local molecular structures to packing domains (61). We focused on molecular and domain packing structures and their dependence on oligomer lengths and the interplay of different relevant forces that control the oligomer film morphology, a key parameter in device optimization. The AFM images for three oligomers (Fig. 4) show that differences in backbone lengths of the oligomers result in distinctly different morphologies in these thin films. The fibrous morphology appearing only in M9 is in stark contrast to those appearing in the M5 and M17 films. After investigating several AFM images of the M9 films, we determined that the fibers have two distinct dimensions. The wider crystalline fibers were roughly 0.8–1.2 μm wide and $>26$ μm long while the thinner fibrils were roughly 80–100 nm in width. The thickness of the fibers was approximately 20 nm. The films of M5 and M17 both show domains without apparent order. The random domains in M5 were approximately 150–300 nm in diameter, while those in M17 were approximately 75–300 nm in size.

In order to investigate the nature of the fiber formation in the M9 films and further understand the forces involved in self-assembly processes, GIXRD was also performed on these films where an x-ray beam strikes the surface of a material at very small angles. A two-dimensional scattering image is collected by an area detector. The scattering angle and, therefore, the scattering vectors ($q$) in reciprocal space are collected in two dimensions. The domain sizes and orientations are thus obtained. The GIXRD patterns for the oligomers can be obtained in different $q$ ranges via grazing incidence wide angle x-ray scattering (GIWAXS) and grazing incidence small angle x-ray scattering (GISAXS) studies. The $d$-spacing is determined by the relationship $d = 2\pi/q$. Here the



Citation: Nano Reviews 2011, 2: 7249 - DOI: 10.3402/nano.v2i0.7249

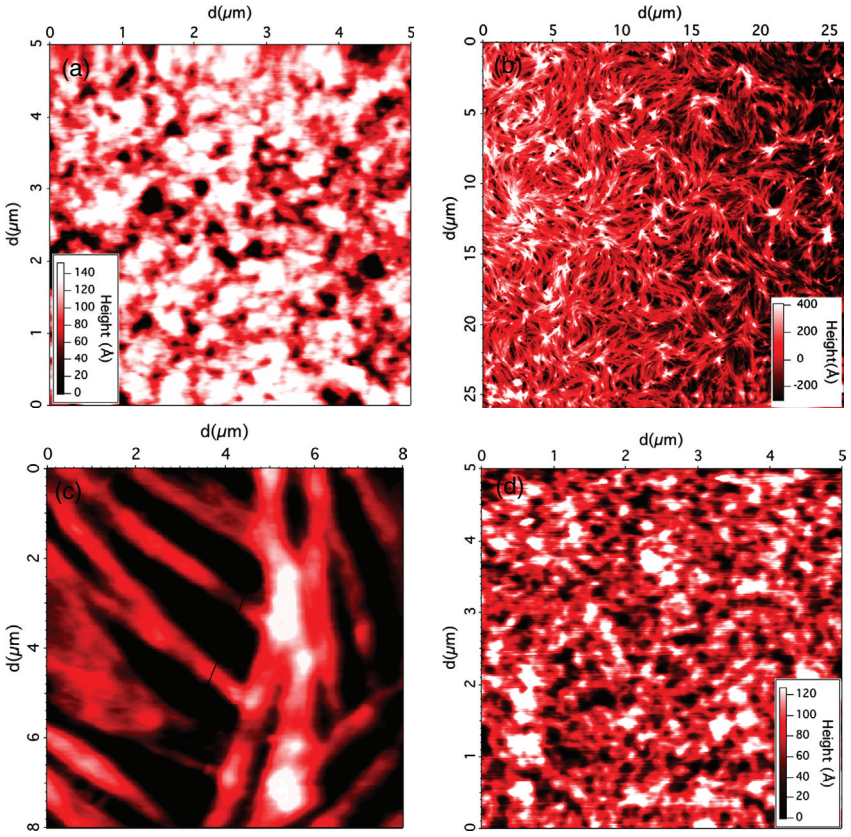


*Fig. 4.* The AFM images of (a) M5, (b,c) M9, and (d) M17. Both M5 and M17 are shown on a 5 μm scale while M9 is shown on two different length scales: 8 μm and 26 μm.

GIWAXS results are discussed first. Only the M9 and M17 films are presented here, because no evidence of any ordering in the M5 films was observed. The M9 and M17 scattering patterns show that the oligomers had an 'edge-on' orientation to have the oligomer backbones parallel but the conjugated backbone planes perpendicular to the substrate, similar to the orientation of hexyl thiophene oligomers and polymers observed previously (67).

The out-of-plane GIWAXS reflections of M9 and M17 were associated with the *d*-spacing of the width of the oligomer backbone including the extended aliphatic side chains, which for convenience is referred to as the 'side chain direction'. This direction corresponds to the (h00) scattering peaks in the GIXRD data (Fig. 5). The position and spacing of these peaks were very similar for the two films, but the M9 showed even and odd (h00) peaks, while M17 only showed even (h00) peaks. Although M9 diffracts signals at the odd-ordered reflections, these peaks were lower in intensity compared to the even-ordered reflections. These out-of-plane diffraction signals were rationalized by adjacent stacking layers with oppositely directed ester-chains, which are attached to the central TT units (61). For example, if one layer's ester chains point toward the substrate, then its neighboring layers have ester chains pointing away from the substrate. The odd-ordered peaks observed in the M9 film originate from a slight break in the adjacent layer symmetry due to the systematic orientation of the ester chains. In the case of M17, the odd-ordered peaks are completely absent. There are increased orientational defects in M17, indicating that the ester chain interactions in the side chain axis are weaker relative to M9, where the assembly is more ordered. Therefore, the forces of the ester chain packing are stronger in the M9 film, while this unit is considered to be a more randomized quasi-defect site in the M17 film. There are fewer ester chains in the M17 oligomer, which weakened the overall interacting forces of the ester chain and, therefore, the packing order in the film. Diffraction features associated with π-stacking along the in-plane direction appeared at $q = 1.61$ Å$^{-1}$ for M9, 1.65 Å$^{-1}$ for M17, or $d = 0.39$ nm and 0.38 nm, respectively. M17 had a greater orientational distribution of π stacking as well, which was indicated by the broad semicircular pattern centered at approximately $q = 1.6$ Å$^{-1}$. This increased isotropic nature of this feature further substantiated the claim that M17 has increased orientational defects relative to M9. In contrast, this feature is more anisotropic in M9, suggesting that M9 has a more epitaxial orientation upon the substrate.

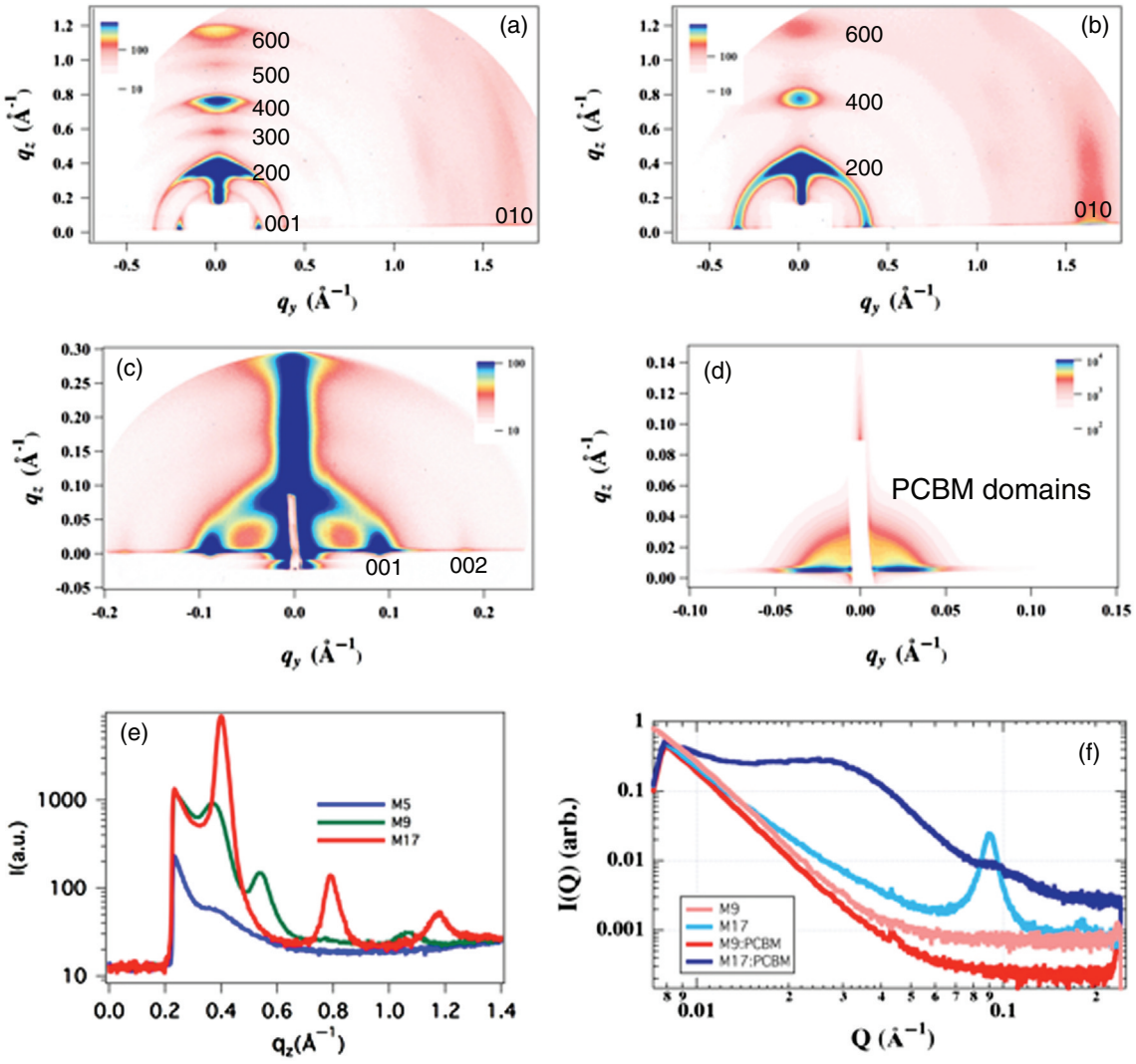


*Fig. 5.* (a,b) The wide angle grazing incidence x-ray scattering images of (a) M9 and (b) M17. The Bragg indices are indicated to the right of or on the peaks. (c,d) The small angle grazing incidence x-ray scattering images of (c) M17 and (d) the M17:PCBM blended film. (e,f) The linecuts of (e) the wider angle and (f) the smaller angle scattering images of the various films. In (e), the change in the degree of order for M5, M9, M17 is monitored by the changes in the scattering of the lamellar 200 Bragg peaks. In (f), the enhancement of the phase separation in M17 compared to M9 is observed.

For the small angle scattering signals, the M17 in-plane signal at $q = 0.0911$ Å$^{-1}$ in the GISAXS image (Fig. 5d) denoted a *d*-spacing of 6.89 nm, which is close to the calculated oligomer backbone length of 6.9 nm. M9 showed an in-plane signal in both GIWAXS and GISAXS at $q = 0.236$ Å$^{-1}$, corresponding to a *d*-spacing of 2.66 nm. This scattering feature corresponds approximately to the length of the M9 backbone. Therefore, the backbones of M17 and M9 both lie parallel to the substrate surface. The M5 diffraction signal (not shown in this review; see Yin and colleagues) (58) shows a lack of regular order, displaying only a single isotropic ring at $q = 0.341$ Å$^{-1}$ ($d = 1.84$ nm) corresponding to the backbone length. No other features were observed, which indicated that the M5 film is highly randomized. The linecut of the three films are shown in Fig. 5e.

Finally, the addition of PCBM to the M9 and M17 oligomer films was investigated using GISAXS to observe the presence of phase-separated domains in the blended films. The linecuts of the GISAXS images for the M9, M9:PCBM, M17, and M17:PCBM polymers are also shown in Fig. 5f. It is well known that the polymers tend to phase separate when blended with PCBM (68). This plot is presented in the log scale to better elucidate the form factors indicating the formation of domains in the films containing PCBM due to phase separation. In these films, the form factor shows a bended curve or a 'knee', which is called the Guinier region. In this region,



Citation: Nano Reviews 2011, **2**: 7249 - DOI: 10.3402/nano.v2i0.7249

the size of the phase separated domains were determined. The neat M9 and M17 films do not have any observable domains in the ~1–50 nm region. The slight curve on the M9 trace does indicate that this film may have larger domains that cannot be recorded in this range, but cannot be confirmed or quantified in the scope of thee experiments. The AFM images of M9 do indicate that very large micron domains were present in this material. In the M17 neat film only shows the ordered peak due to the backbone chain. When PCBM is added to the M17 film, a 6 nm phase separated domain was observed while the M9 does not show a substantial change in the GISAXS form factor. The rationale for this lack of domain formation was that the intermolecular forces in M9 are much stronger, so there is no interaction of the M9 with the PCBM material. The overall solar cell device efficiency was extremely low for the M9 film. This low efficiency is attributed to the lack of PCBM and polymer interaction in the films. If M9 form micron domains in the film, and PCBM cannot intercalate in between these films, then there will be very little exciton splitting in the material.

These results enabled us to form the following conclusion: the intermolecular forces of the M5 oligomer are the strongest. In fact, they are strong enough to overwhelm the interaction with the substrate surface. The M9 is an intermediate case where the interactions no longer out compete the surface tension and, therefore, the M9 spreads out over the substrate. However, it does not spread out uniformly and instead forms aggregates with ester chains regularly oriented toward each other in adjacent stacking layers. In the M17 case, the ester chain contributions are the weakest and, therefore, the ester interactions are not strong enough to prevent the oligomers from exhibiting orientational defects along the side chain axis. At the same time, the opposite trend takes place in the π-stacking and aliphatic chain interactions, which are strengthened with increasing numbers of hexylthiophene monomers in the backbone. Therefore, M17 has the strongest π-stacking and aliphatic chain interactions, followed by M9, and lastly M5.

## 2. Oligomer and polymer comparisons: a spectral, morphological, and dynamic investigation

### 2.1. Optical properties

To investigate the difference of oligomer BHJ films compared to their polymer counterparts, two species,

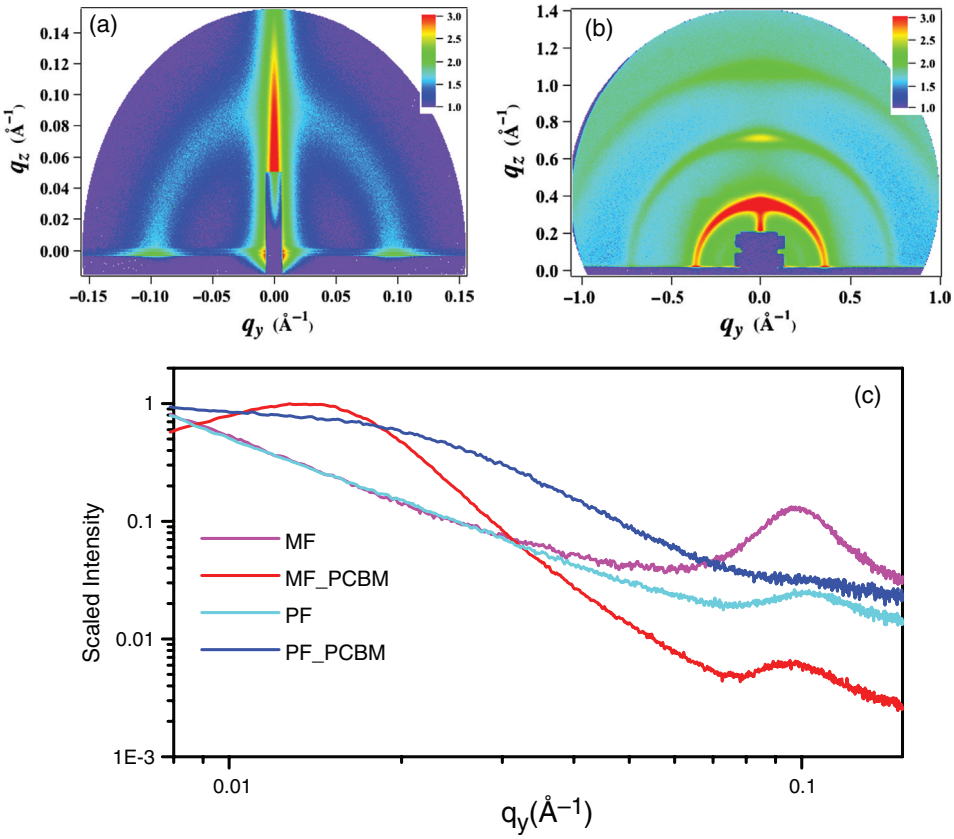


*Fig. 6.* (a) GISAXS and (b) GIWAXS images of MF. (c) Horizontal linecuts of the GISAXS images of the following films: MF, MF:PCBM, PF, PF:PCBM. The enhanced order of the phase separation in the MF:PCBM film compared to the PF:PCBM film is shown by the lower $q$ values and smaller width of the Guinier region.

MF and PF, were also fabricated (62). Their structures are shown in Fig. 2. These species are structurally similar to the M series oligomers. The UV-vis absorption spectra of MF and PF were measured in dilute chlorobenzene solutions as well as in spin-coated films and are shown in Fig. 3. The bandgap of MF and PF was about 0.20 eV smaller than that of P3HT, which further demonstrated that the incorporation of the TT moiety into the oligomer or polymer backbone significantly lowered the material bandgap. The enhanced interchain interaction in the films can cause a significant red shift in the absorption spectra relative to that of the solution samples (69). When the MF and PF films were compared, the latter showed a slightly larger red-shifted absorption as a result of increasing conjugation length.

### 2.2. Molecular packing structures: higher order in the oligomer films

Fig. 6 shows the GISAXS and GIWAXS images of the MF film. The scattering profiles for $q = 0.006$–$0.155$ Å$^{-1}$ are shown in Fig. 6a, while Fig. 6b shows the scattering profile for $q = 0.14$–$1.00$ Å$^{-1}$. The domain spacing was obtained by the relationship $d = 2\pi/q$. In Fig. 6a, the broad ring corresponds to an average $d$-spacing of 6.45 nm and is comparable to the thiophene chain length in the MF molecule. Higher order peaks were also observed, which indicates lamellar order in the film. Similar peaks were observed in the M17 film. Although this $d$-spacing was present in all four samples (MF, MF:PCBM, PF, and PF:PCBM), it was the most prominent in the MF sample. The horizontal line profiles of images of the four thin film samples are shown in Fig. 6c. The Guinier region was also analyzed for these samples in a similar fashion to the analysis of the M17 films discussed in the previous section. For the MF:PCBM film, the Guinier region represents a larger domain than in the PF:PCBM sample. The form factor of the MF:PCBM film indicated that the domains are more ordered and closer together in this sample. These experiments indicate that there are larger and more ordered structures in the MF:PCBM film compared to the PF:PCBM film, which will lower the exciton splitting efficiency due to the exciton diffusion length limit in the films.

### 2.3. Charge separation (CS) and charge recombination (CR) dynamics of MF/PCBM and PF/PCBM films: effects of domain size and crystallinity on the charge carrier kinetics

The ultrafast transient absorption spectroscopy probes the dynamics of fundamental processes in PV materials such as exciton generation, CS, and charge recombination (CR). The CS and CR dynamics of MF:PCBM and PF:PCBM were measured by ultrafast optical transient absorption (TA) spectroscopy with an excitation wavelength of 600 nm. A broad absorption from 670–1060 nm that was found in the TA spectra of the PF:PCBM was observed and was attributed to the cation absorption of PF after charge transfer from PF to PCBM. The transient spectra of MF:PCBM show the cation absorption of MF extends from 620 to 1040 nm. Therefore, the CS and CR dynamics in MF:PCBM or PF:PCBM films were monitored by the kinetic traces at a probe wavelength of 700 nm to record the formation and decays rates of the cationic state in both films. Fig. 7 shows the kinetic traces of MF:PCBM and PF:PCBM films monitored at 700 nm. The MF:PCBM has a faster CS rate and slower CR rate than PF:PCBM. However, the cation yield of PF:PCBM at 3 ns is about 70% higher than that of MF:PCBM. This suggested that the free charge carriers generated in PF:PCBM is much higher than MF:PCBM. As a result, the PF:PCBM cell showed a higher efficiency than the MF:PCBM cell although the CS and CR dynamics is more favorable for the MF:PCBM cell. The low charge carrier yield in the MF:PCBM film was correlated with the lower exciton splitting efficiency due to the crystalline domains with sizes exceeding the exciton diffusion length in the film as was suggested in the AFM and GIXS results.

### 2.4. Photovoltaic properties of MF and PF in relation to their physical properties in films

The solar cells containing MF or PF were fabricated with the structure of ITO/PEDOT-PSS/polymer:PCBM/Al, and the PV performance measurements were carried out under ambient atmosphere. The current density of the PF:PCBM solar cell reaches to 10.2 mA/cm$^2$, which is comparable to reported P3HT:PCBM devices (70). However, a slightly lower open circuit voltage (0.56 V) and a low fill factor (0.4) limits its efficiency to 2.4%. The solar cells prepared from MF are inferior in their physical performance to the PF devices, with a current density of $\sim$70% of the PF solar cells (7.42 mA/cm$^2$), comparable open circuit voltage (0.54 V), and fill factor (0.36) to yield an overall efficiency of 1.46%. The considerably lower efficiency of the MF films is once again rationalized by the larger and more ordered domains in the MF films.

## Summary and perspective

In the interdisciplinary effort to optimize small molecules for solar cell applications, a variety of molecular and bulk properties have been investigated and fine-tuned. However, we have discussed how this task is made difficult by the often competing optimization rules for these properties. Competition between exciton diffusion distance and active layer thickness for sufficient optical absorption necessitated the engineering of bulk heterojunction morphologies; but, in turn, this required a substantial effort first to functionalize the electron acceptor PCBM, and secondly to optimize the complicated



Citation: Nano Reviews 2011, 2: 7249 - DOI: 10.3402/nano.v2i0.7249

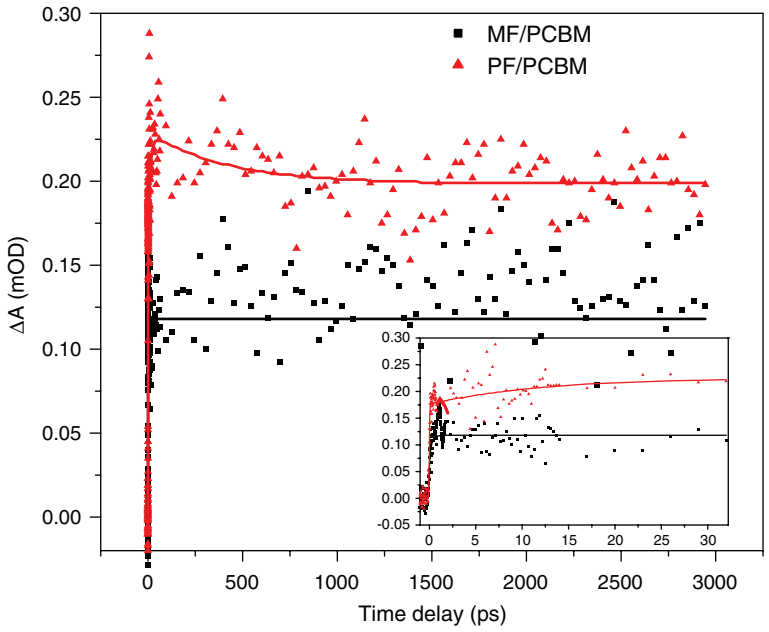


*Fig. 7.* The transient kinetics of the MF:PCBM and PF:PCBM blended films. The same traces with a smaller window are shown in the inset. The kinetics traces measure the rise and decay of the cationic state in the oligomer or polymer species.

morphology inherent in this device architecture. Finding the conditions for maximal PCE is therefore a subtle negotiation requiring an acutely tuned set of optimal conditions, because these competing considerations must be satisfied simultaneously. The investigation of oligothiophene derivatives has improved our understanding of such processes. The higher degree of processing abilities has made oligothiophenes and attractive candidate as donor materials in OPV devices. The ability to systematically alter the structure of these materials has also enabled us to better understand the fundamental processes in such materials. Through the study of the interplay of morphology, energetics, kinetics, as well as the optimization of fabrication techniques, we are converging on mass marketable solar cell efficiencies composed of these kinds of materials.

Great interests in OPV research holds on the promise of low-cost, readily manufacturable alternatives to traditional inorganic systems for producing solar electricity. However, the main present obstacles in OPV commercialization are still low PCE and limited operating lifetime in OPV devices. Based on impressive advances recently, power conversion efficiencies as high as 10–12% may be achievable if crucial scientific understanding challenges can be surmounted. These challenges involve fundamental material issues of how light interacts with soft matter, how excitons diffuse and split, and how holes and electrons are transported in the soft matter then extracted by both transparent and metallic hard matter electrodes. All these issues are closely related to nanoscale morphology in organic materials. As new materials such as graphene and carbon nanotubes, and new cell structures such as tandem cells emerge for OPV applications, the cost of OPV devices can be further reduced and the operating time could be further extended. Although OPV devices will unlikely replace their counterparts made from inorganic materials in the near future, they have their niche in solar electricity generation. We can envision that the so called 'solar paint' may be realized in the next decade, which can harvest solar photons in many different ways using light, inexpensive, flexible and renewable materials to equip building walls, windows, fabrics, and other areas exposed to sunlight.

## Conflict of interest and funding

There is no conflict of interest in the present study for any of the authors.

## Acknowledgements

This research is supported by the ANSER Center, an Energy Frontier Research Center funded by the US Department of Energy, Office of Science, Office of Basic Energy Sciences under Award Number DE-SC0001059 and the Division of Chemical Sciences, Office of Basic Energy Sciences, the US Department of Energy under contract DE-AC02-06CH11357 (for L. X. C.). The gift from Intel Corporation for a part of the research is greatly appreciated. The authors would also like to acknowledge our long-time collaborators from Professor Luping Yu's group at the University of Chicago who are responsible for the materials synthesis in a number of systems included in this review. We would also like to thank Drs. David J. Gosztola and Gary P. Wiederrecht for their help in some optical transient absorption measurements conducted at the Center for Nanoscale Materials at Argonne National Laboratory; Drs. Joseph W. Strzalka, Byeondu Lee, and Sonke Seifert for their help and collaboration in the x-ray scattering experiments at the

Advanced Photon Source also at Argonne National Laboratory. The use of the Advanced Photon Source and the facilities at the Center for Nanoscale Materials were supported by the US Department of Energy, Office of Science, Office of Basic Energy Sciences under Contract No. DE-AC02-06CH11357.

## References


1. Tang CW. 2-Layer organic photovoltaic cell. Appl Phys Lett 1986; 48: 183–5.
2. Yu G, Gao J, Hummelen JC, Wudl F, Heeger AJ. Polymer photovoltaic cells: enhanced efficiencies via a network of internal donor-acceptor heterojunction. Science 1995; 270: 1789–91.
3. Peumans P, Uchida S, Forrest SR. Efficient bulk heterojunction photovoltaic cells using small-molecular-weight organic thin films. Nature 2003; 425: 158–62.
4. Sariciftci NS, Smilowitz L, Heeger AJ, Wudl F. Photoinduced electron-transfer from a conducting polymer to buckminsterfullerene. Science 1992; 258: 1474–6.
5. Hains AW, Liang Z, Woodhouse MA, Gregg BA. Molecular semiconductors in organic photovoltaic cells. Chem Rev 2010; 110: 6689–735.
6. Rand BP, Genoe J, Heremans P, Poortmans J. Solar cells utilizing small molecular weight organic semiconductors. Prog Photovolt: Res Appl 2007; 15: 659–76.
7. Baba H, Chitoku K, Nitta K. Photoelectric phenomena with copper phthalocyanine. Nature 1956; 177: 672.
8. Kronik L, Shapira Y. Surface photovoltage phenomena: theory, experiment, and applications. Surf Sci Rep 1999; 37: 1–206.
9. Hennebicq E, Pourtois G, Scholes GD, Herz LM, Russell DM, Silva C, et al. Exciton migration in rigid-rod conjugated polymers: an improved Förster model. J Am Chem Soc 2005; 127: 4744–62.
10. Schwenn PE, Gui K, Nardes AM, Krueger KB, Lee KH, Mutkins K, et al. A small molecule non-fullerene electron acceptor for organic solar cells. Adv Energy Mater 2010; 1: 73–81.
11. Shirota Y. Organic materials for electronic and optoelectronic devices. J Mater Chem 2000; 10: 1–25.
12. Wei G, Wang S, Renshaw K, Thompson ME, Forrest SR. Solution-processed squaraine bulk heterojunction photovoltaic cells. Acs Nano 2010; 4: 1927–34.
13. 'Heliatek and IAPP production-relevant efficiency record for organic photovoltaic cells', http://www.heliatek.com/news-19, October 11, 2010
14. 'Konarka's Power Plastic Achieves World Record 8.3% Efficiency Certification from National Energy Renewable Laboratory (NREL) http://www.konarka.com/index.php/site/pressreleasedetail/konarkas_power_plastic_achieves_world_record_83_efficiency_certification_fr, November 29, 2010
15. Peumans P, Bulovic V, Forrest SR. Efficient photon harvesting at high optical intensities in ultrathin organic double-heterostructure photovoltaic diodes. Appl Phys Lett 2000; 76: 2650–2.
16. Hiramoto M, Fujiwara H, Yokoyama M. 3-Layered organic solar-cell with a photoactive interlayer of codeposited pigments. App Phys Lett 1991; 58: 1062–4.
17. Vogel JO, Salzmann I, Duhm S, Oehzelt M, Rabe JP, Koch N. Phase-separation and mixing in thin films of co-deposited rod-like conjugated molecules. J Mater Chem 2010; 20: 4055–66.
18. Pandey R, Holmes RJ. Graded donor-acceptor heterojunctions for efficient organic photovoltaic cells. Adv Mater 2010; 22: 5301–5.
19. Liang FS, Shi F, Fu YY, Wang LF, Zhang XT, Xie ZY, et al. Donor-acceptor conjugates-functionalized zinc phthalocyanine: towards broad absorption and application in organic solar cells. Sol Energy Mater Sol Cells 2010; 94: 1803–8.
20. Ofuji M, Inaba K, Omote K, Hoshi H, Takanishi Y, Ishikawa K, et al. Grazing incidence in-plane x-ray diffraction study on oriented copper phthalocyanine thin films. Jpn J Appl Phys 2002; 41: 5467–71.
21. Law KY. Organic photoconductive materials – recent trends and developments. Chem Rev 1993; 93: 449–86.
22. Krebs FC, Fyenbo J, Jorgensen M. Product integration of compact roll-to-roll processed polymer solar cell modules: methods and manufacture using flexographic printing, slot-die coating and rotary screen printing. J Mater Chem 2010; 20: 8994–9001.
23. Petritsch K, Dittmer JJ, Marseglia EA, Friend RH, Lux A, Rozenberg GG, et al. Dye-based donor/acceptor solar cells. Sol Energy Mater Sol Cells 2000; 61: 63–72.
24. Mutolo KL, Mayo EI, Rand BP, Forrest SR, Thompson ME. Enhanced open-circuit voltage in subphthalocyanine/C-60 organic photovoltaic cells. J Am Chem Soc 2006; 128: 8108–9.
25. Ma B, Woo CH, Miyamoto Y, Frechet JMJ. Solution processing of a small molecule, subnaphthalocyanine, for efficient organic photovoltaic cells. Chem Mater 2009; 21: 1413–7.
26. Silvestri F, Irwin MD, Beverina L, Facchetti A, Pagani GA, Marks TJ. Efficient squaraine-based solution processable bulk-heterojunction solar cells. J Am Chem Soc 2008; 130: 17640–1.
27. Mayerhöffer U, Deing K, Gruß K, Braunschweig H, Meerholz K, Würthner F. Outstanding short-circuit currents in BHJ solar cells based on NIR-absorbing acceptor-substituted squaraines. Angew Chem Int Ed 2009; 48: 8776–9.
28. Wei G, Lunt RR, Sun K, Wang S, Thompson ME, Forrest SR. Efficient, ordered bulk heterojunction nanocrystalline solar cells by annealing of ultrathin squaraine thin films. Nano Letters 2010; 10: 3555–9.
29. Wei G, Wang S, Sun K, Thompson ME, Forrest SR. Solvent-annealed crystalline squaraine: PC70BM (1:6) solar cells. Adv Energy Mater 2011; 1: 184–7.
30. Forrest SR. Ultrathin organic films grown by organic molecular beam deposition and related techniques. Chem Rev 1997; 97: 1793–896.
31. Peumans P, Yakimov A, Forrest SR. Small molecular weight organic thin-film photodetectors and solar cells. J Appl Phys 2003; 93: 3693–723.
32. Chen L, Xiao S, Yu L. Dynamics of photoinduced electron transfer in a molecular donor-acceptor quartet. J Phys Chem B 2006; 110: 11730–8.
33. Guo JC, Liang YY, Xiao SQ, Szarko JM, Sprung M, Mukhopadhyay MK, et al. Structure and dynamics correlations of photoinduced charge separation in rigid conjugated linear donor-acceptor dyads towards photovoltaic applications. New J Chem 2009; 33: 1497–507.
34. El-Khouly ME, Ito O, Smith PM, D'Souza F. Intermolecular and supramolecular photoinduced electron transfer processes of fullerene-porphyrin/phthalocyanine systems. J Photoch Photobio C 2004; 5: 79–104.
35. Sommer M, Huettner S, Thelakkat M. Donor-acceptor block copolymers for photovoltaic applications. J Mater Chem 2010; 20: 10788–97.
36. Wasielewski MR. Photoinduced electron-transfer in supramolecular systems for artificial photosynthesis. Chem Rev 1992; 92: 435–61.
37. Kroto HW, Heath JR, Obrien SC, Curl RF, Smalley RE. C-60 – buckminsterfullerene. Nature 1985; 318: 162–3.
38. Sariciftci NS, Braun D, Zhang C, Srdanov VI, Heeger AJ, Stucky G, et al. Semiconducting polymer-buckminsterfullerene heterojunctions – diodes, photodiodes, and photovoltaic cells. Appl Phys Lett 1993; 62: 585–7.




Citation: Nano Reviews 2011, **2**: 7249 - DOI: 10.3402/nano.v2i0.7249

39. Peumans P, Forrest SR. Very-high-efficiency double-heterostructure copper phthalocyanine/C-60 photovoltaic cells. Appl Phys Lett 2001; 79: 126–8.
40. Sension RJ, Szarka AZ, Smith GR, Hochstrasser RM. Ultrafast photoinduced electron-transfer to C60. Chem Phys Lett 1991; 185: 179–83.
41. Hummelen JC, Knight BW, Lepeq F, Wudl F, Yao J, Wilkins CL. Preparation and characterization of fulleroid and methanofullerene derivatives. J Org Chem 1995; 60: 532–8.
42. Wienk MM, Kroon JM, Verhees WJH, Knol J, Hummelen JC, van Hal PA, et al. Efficient methano[70]fullerene/mdmo-ppv bulk heterojunction photovoltaic cells. Angew Chem Int Ed 2003; 42: 3371–5.
43. Allemand PM, Koch A, Wudl F, Rubin Y, Diederich F, Alvarez MM, et al. 2 different fullerenes have the same cyclic voltammetry. J Am Chem Soc 1991; 113: 1050–1.
44. Cheng Y, Hsieh C, Heldots Y. Combination of indene-c60 bisadduct and cross-linked fullerene interlayer leading to highly efficient inverted polymer solar cells. J Am Chem Soc 2010; 132: 17381–3.
45. de Bettignies R, Nicolas Y, Blanchard P, Levillain E, Nunzi JM, Roncali J. Planarized star-shaped oligothiophenes as a new class of organic semiconductors for heterojunction solar cells. Adv Mater 2003; 15: 1939.
46. Wynands D, Mannig B, Riede M, Leo K, Brier E, Reinold E et al. Organic thin film photovoltaic cells based on planar and mixed heterojunctions between fullerene and a low bandgap oligothiophene. J Appl Phys 2009; 106: 054509.
47. Roncali J. Synthetic principles for bandgap control in linear pi-conjugated systems. Chem Rev 1997; 97: 173–205.
48. Dennler G, Scharber MC, Brabec CJ. Polymer-fullerene bulk-heterojunction solar cells. Adv Mater 2009; 21: 1323–38.
49. Walker B, Kim C, Nguyen T-Q. Small molecule solution-processed bulk heterojunction solar cells. Chem Mater 2011; 23: 470–82.
50. Bundgaard E, Krebs FC. Low band gap polymers for organic photovoltaics. Sol Energy Mater Sol Cells 2007; 91: 954–85.
51. Walker B, Tamayo AB, Dang X-D, Zalar P, Seo JH, Garcia A, et al. Nanoscale phase separation and high photovoltaic efficiency in solution-processed, small-molecule bulk heterojunction solar cells. Adv Funct Mater 2009; 19: 3063–9.
52. Walker B, Tamayo A, Duong DT, Dang X-D, Kim C, Granstrom J, et al. A systematic approach to solvent selection based on cohesive energy densities in a molecular bulk heterojunction system. Adv Energy Mater 2011; 1: 221–9.
53. Cai X, Burand MW, Newman CR, Filho DADS, Pappenfus TM, Bader MM, et al. N- and p-channel transport behavior in thin film transistors based on tricyanovinyl-capped oligothiophenes. J Phys Chem B 2006; 110: 14590–7.
54. Pappenfus TM, Burand MW, Janzen DE, Mann KR. Synthesis and characterization of tricyanovinyl-capped oligothiophenes as low-band-gap organic materials. Org Lett 2003; 5: 1535–8.
55. Milian B, Orti E, Hernandez V, Navarrete JTL, Otsubo T. Spectroscopic and theoretical study of push-pull chromophores containing thiophene-based quinonoid structures as electron spacers. J Phys Chem B 2003; 107: 12175–83.
56. Muhammad FF, Sulaiman K. Photovoltaic performance of organic solar cells based on dh6t/pcbm thin film active layers. Thin Solid Films 2011; 519: 5230–3.
57. Wynands D, Levichkova M, Leo K, Uhrich C, Schwartz G, Hildebrandt D, et al. Increase in internal quantum efficiency in small molecular oligothiophene: C-60 mixed heterojunction solar cells by substrate heating. Appl Phys Lett 2010; 97: 073503.
58. Yin B, Yang L, Liu Y, Chen Y, Qi Q, Zhang F, et al. Solution-processed bulk heterojunction organic solar cells based on an oligothiophene derivative. Appl Phys Lett 2010; 97: 023303.
59. Uhrich CL, Schwartz G, Maennig B, Gnehr WM, Sonntag S, Erfurth O, et al. Efficient and long-term stable organic vacuum deposited tandem solar cells. Organic Photonics IV 2010; 7722: 77220G.
60. Szarko JM, Rolczynski BS, Guo J, Liang Y, He F, Mara MW et al. Electronic processes in conjugated diblock oligomers mimicking low band-gap polymers: experimental and theoretical spectral analysis. J Phys Chem B 2010; 114: 14505–13.
61. Rolczynski BS, Szarko JM, Lee B, Strzalka J, Guo JC, Liang YY, et al. Length-dependent self-assembly of oligothiophene derivatives in thin films: implications in photovoltaic material fabrications. J Mater Res 2011; 26: 296–305.
62. Liang VY, Feng DQ, Guo JC, Szarko JM, Ray C, Chen LX et al. Regioregular oligomer and polymer containing thieno[3,4-b]thiophene moiety for efficient organic solar cells. Macromolecules 2009; 42: 1091–8.
63. Moet DJD, Koster LJA, de Boer B, Blom PWM. Hybrid polymer solar cells from highly reactive diethylzinc: MDMO-PPV versus P3HT. Chem Mater 2007; 19: 5856–61.
64. Zou JH, Khondaker SI, Huo Q, Zhai L. A general strategy to disperse and functionalize carbon nanotubes using conjugated block copolymers. Adv Funct Mater 2009; 19: 479–83.
65. Meier H, Stalmach U, Kolshorn H. Effective conjugation length and uv/vis spectra of oligomers. Acta Polym 1997; 48: 379–84.
66. Cates NC, Gysel R, Dahl JEP, Sellinger A, McGehee MD. Effects of intercalation on the hole mobility of amorphous semiconducting polymer blends. Chem Mater 2010; 22: 3543–8.
67. Yang HH, LeFevre SW, Ryu CY, Bao ZN. Solubility-driven thin film structures of regioregular poly(3-hexyl thiophene) using volatile solvents. Appl Phys Lett 2007; 90: 172116.
68. Chiu MY, Jeng US, Su CH, Liang KS, Wei KH. Simultaneous use of small- and wide-angle x-ray techniques to analyze nanometerscale phase separation in polymer heterojunction solar cells. Adv Mater 2008; 20: 2573–8.
69. Politis JK, Nemes JC, Curtis MD. Synthesis and characterization of regiorandom and regioregular poly(3-octylfuran). J Am Chem Soc 2001; 123: 2537–47.
70. Reyes-Reyes M, Kim K, Dewald J, Lopez-Sandoval R, Avadhanula A, Curran S, et al. Meso-structure formation for enhanced organic photovoltaic cells. Org Lett 2005; 7: 5749–52.



***Lin X. Chen**
Department of Chemistry Argonne Northwestern Solar Energy Research (ANSER) Center
Northwestern University
2145 Sheridan Road
Evanston, IL 60208, USA
Tel: +(630) 252 3533
Email: lchen@anl.gov or l-chen@northwestern.edu